International Journal of Engineering Technology and Management Sciences
Website: ijetms.in Issue: 3 Volume No.8 May - June – 2024
DOI:10.46647/ijetms.2024.v08i03.079 ISSN: 2581-4621

Design, fabrication and performance assessment of a solar-assisted three-wheel electric scooter for short-distance campus mobility

B. Srihari[a,*], C. Yaswanth Kumar[a], D. Siddiq[a], D. Vamsidhar Reddy[a], E. Giridhar Kumar[a], G. Yugandhar Chowdary[a]
[a] *Department of Mechanical Engineering, K.S.R.M. College of Engineering (Autonomous), Kadapa 516 005, Andhra Pradesh, India*
* Corresponding author.:bsh@ksrmce.ac.in

Abstract
Battery electric two- and three-wheelers are displacing internal-combustion vehicles rapidly in Indian cities, but the environmental benefit of that transition is bounded by the carbon intensity of the grid that charges them. On-board photovoltaic (PV) generation offers a partial decoupling for low-power personal mobility, where the deck area available for a module is a meaningful fraction of the daily energy demand. This paper reports the complete design chain, fabrication and performance assessment of a solar-assisted three-wheel electric scooter intended for short-distance movement inside campuses, airports and industrial premises. Candidate structural materials were screened and AISI 1020 square hollow section was selected on the basis of weldability, cost and adequacy of strength for the 114 kg design gross mass. Tractive resistance analysis for a rolling resistance coefficient of 0.0046 gives a road-load torque of 0.83 N m and a total starting torque requirement of 9.27 N m, met by a 250 W, 24 V brushless DC motor driving the rear axle through an 11:28 chain reduction. A 24 V lithium-ion pack sized at 14.4 A h delivers a continuous full-power runtime of 0.83 h at the 10.42 A draw, and conductor sizing against a 2% permissible voltage drop yields AWG 10 copper. The prototype was fabricated by gas metal arc welding on a 900 mm × 300 mm rectangular frame and instrumented with a PWM motor controller and a PV charge controller. Energy accounting indicates that a 30–50 Wp deck-mounted module at the site irradiance of approximately 5.5 kWh m^{-2} day^{-1} recovers 140–234 W h per day, equivalent to 41–68% of the pack energy. Discrepancies between the design case and the as-built machine, principally in sprocket ratio, wheel diameter and installed pack capacity, are quantified and their effect on attainable road speed is discussed.
Keywords: Solar-assisted electric vehicle; Brushless DC motor; Photovoltaic charging; Lithium-ion battery; Personal mobility; Prototype fabrication

1. Introduction

Road transport is among the fastest-growing sources of greenhouse gas emissions and of urban air pollution in India, and a disproportionate share of that burden is generated by short trips. Movement inside large campuses, airports, warehouses, hospital complexes and industrial estates is dominated by journeys of one to five kilometres at speeds well below 15 km h^{-1}, a duty cycle for which a conventional petrol two-wheeler is thermodynamically and economically inefficient. Battery electric personal mobility vehicles are a natural substitute for this class of trip, and falling lithium-ion cell prices together with the entry of established manufacturers have made them commercially viable.

The environmental case for a battery electric vehicle is nevertheless conditional. A scooter charged from a grid dominated by coal-fired generation displaces tailpipe emissions to the generating station rather than eliminating them. For low-power vehicles the imbalance between available surface area and energy demand is unusually favourable: a scooter deck of the order of 0.3 m^2 can carry a photovoltaic module whose daily yield is a substantial fraction of the traction energy actually consumed. On-board photovoltaic assistance is therefore worth evaluating for this vehicle class, even though it is of marginal value for passenger cars.

Published student and small-scale work on campus electric vehicles has concentrated either on the mechanical layout of the frame and drivetrain or on the electrical control architecture, and the two are seldom carried through a single consistent design chain. Reports that do include photovoltaic charging frequently omit the energy accounting that would establish whether the module contributes materially to range. A second recurring weakness is that scaled prototypes are described without reconciling the as-built machine against the parameters used in the design calculations, so the reader cannot judge how far the reported performance follows from the analysis.

This paper addresses both gaps. It reports the design, fabrication and assessment of a solar-assisted three-wheel electric scooter, carried from the tractive load through motor and battery selection, conductor sizing and drivetrain ratio to the fabricated prototype. The specific objectives were: (i) to select a frame material and joining process appropriate to a 114 kg design gross mass at minimum cost; (ii) to size the traction motor, battery and conductors against a 10 km h^{-1} target top speed; (iii) to fabricate a working prototype using workshop-available processes; and (iv) to quantify the energy contribution of on-board photovoltaic charging and the deviation of the as-built machine from the design case.

2. Related work

A cluster of prototype studies on human- and electrically-powered personal mobility devices provides the immediate context for this work. Ajan et al. [1] and Deshmukh et al. [4] described walking-bike configurations in which rider motion is converted to propulsion through a treadmill belt, establishing the frame geometry and centre-of-gravity constraints that a stand-on machine must satisfy. Gajbhiye et al. [2], Barade et al. [3] and Bondre et al. [7] reported treadmill-cycle variants and documented chain-drive layouts and sprocket ratios for low-speed transmission of modest torque. Ahire et al. [5] and Ansari et al. [6] extended the same architecture with electrical assistance and reported the practical difficulties of mounting a motor and battery on a lightweight tubular frame without compromising stability.

Two conclusions recur across these studies. First, a delta wheel configuration with a single steered front wheel and a driven rear pair provides adequate lateral stability at low speed without the complexity of a differential, provided the centre of gravity is kept low by a negative approach angle. Second, hub or shaft-mounted brushless DC motors are preferred over permanent-magnet DC machines for this duty because of their higher starting torque and power-to-weight ratio, despite requiring an electronic commutation stage.

On the commercial side, the EV Rider Stand N Ride offers a useful benchmark. It uses a 500 W, 24 V outrunner hub motor in a front-wheel-drive delta configuration with a lithium-ion pack, achieves approximately 15 mph with a 15–20 mile range, and disassembles into components of which the heaviest is 43 lb. Machines of this type demonstrate the market viability of the configuration but remain expensive; Segway and comparable manufacturers were unable to reach break-even volumes on campus vehicles at their launch price points, which motivates the low-cost fabrication approach adopted here. Market forecasts published in the mid-2010s projected cumulative global sales of electric motorcycles and scooters of the order of 55 million units over 2015–2024 [8], and three-wheel electric scooters for short-distance mobility were introduced on a trial basis at the Mysore Palace during the 2016 Dussehra season, indicating early institutional interest in exactly the application addressed here.

None of the reviewed prototypes integrates on-board photovoltaic generation with a documented energy balance, and none reports the conductor sizing or the reconciliation of design and as-built parameters presented in Sections 4 and 6.

3. Materials and methods

3.1. Design methodology

The design proceeded iteratively from a statement of objectives to a final frame. Conceptual sketches and a solid model were developed in parallel with material screening; a cross-section was

DOI:10.46647/ijetms.2024.v08i03.079 ISSN: 2581-4621

then selected against combined factor-of-safety and weight criteria, and further iterations on the frame were checked by finite element and ergonomic analysis before the geometry was frozen for fabrication. Because the full-size machine proved infeasible within the available budget and workshop capability, a scaled-down prototype was built and the design parameters were adjusted accordingly; the consequences of that rescaling are quantified in Section 6.

3.2. Structural material selection

Three candidate materials were screened for the frame: AISI 1020 low-carbon steel, AISI 4130 chromium-molybdenum alloy steel, and carbon-fibre-reinforced polymer (CFRP).

AISI 1020 is a low-hardenability carbon steel with a Brinell hardness of 119–235 and a tensile strength of 410–790 MPa. Its low carbon content gives high machinability, high ductility and good weldability, and it accepts all common welding processes in the cold-drawn or turned-and-polished condition. Its composition is given in Table 1.

Table 1. Chemical composition of AISI 1020 low-carbon steel.

Element	**Content (%)**
Carbon, C	0.17–0.230
Iron, Fe	99.08–99.53
Manganese, Mn	0.30–0.60
Phosphorus, P	≤ 0.040
Sulfur, S	≤ 0.050

AISI 4130 contains chromium and molybdenum as strengthening agents and responds far better to heat treatment than a plain carbon steel, while retaining good weldability on account of its low carbon content. It is normalised at 871 °C and oil-quenched, heat-treated between 899 and 927 °C, annealed at 843 °C followed by air cooling at 482 °C, and tempered between 399 and 566 °C depending on the strength required. Its composition is given in Table 2.

Table 2. Chemical composition of AISI 4130 alloy steel.

Element	**Content (%)**
Iron, Fe	97.03–98.22
Chromium, Cr	0.80–1.10
Manganese, Mn	0.40–0.60
Carbon, C	0.280–0.330
Silicon, Si	0.15–0.30
Molybdenum, Mo	0.15–0.25
Sulfur, S	0.040
Phosphorus, P	0.035

CFRP offers the highest specific strength and stiffness of the three and would minimise kerb mass, but it cannot be joined by welding, requires bonded or bolted joints with careful load introduction, and its cost per unit length is an order of magnitude above that of mild steel tube.

AISI 1020 square hollow section was selected. At the 114 kg design gross mass the strength of the alloy steel is not required, the cost premium of CFRP is not recoverable, and weldability is decisive because the entire frame is fabricated in a general-purpose workshop. The section chosen was 25.4 mm × 25.4 mm (1 in × 1 in) square hollow tube.

3.3. Joining process selection

International Journal of Engineering Technology and Management Sciences
Website: ijetms.in Issue: 3 Volume No.8 May - June – 2024
DOI:10.46647/ijetms.2024.v08i03.079 ISSN: 2581-4621

Welding processes were screened against the joint geometry, the section thickness, the need for positional welding on an assembled frame, and the equipment available. Gas metal arc welding (GMAW), in its metal inert gas (MIG) variant, was selected. GMAW strikes an arc between a continuously fed consumable wire electrode and the workpiece under a shielding gas delivered through the gun, and operates from a constant-voltage direct-current source. It is faster than shielded metal arc welding on thin section, produces little slag, and is readily applied in the positions required to close a rectangular frame with all sides welded. The alternatives were rejected on the grounds of speed (oxy-acetylene), electrode changeover and slag removal (shielded metal arc), or capital cost and the need for a highly skilled operator (gas tungsten arc).

3.4. Powertrain component selection

Two motor technologies were compared for the traction duty, as summarised in Table 3.

Table 3. Comparison of BLDC and PMDC machines for the traction duty.

Attribute	BLDC motor	PMDC motor
Starting torque	High	Low
Mass	Light	Heavy
Speed range	High rpm	Low rpm
Efficiency	Higher	Lower
Commutation	Electronic	Mechanical (brushes)

The brushless machine was selected. Starting torque governs the design point for a vehicle that must move a 114 kg gross mass from rest on a level surface, and the absence of a commutator removes the principal wear item and the associated maintenance requirement.

Two battery chemistries were compared, as summarised in Table 4.

Table 4. Comparison of lithium-ion and lead-acid chemistries.

Attribute	Lithium-ion	Lead-acid
Current density	High	Low
Mass	Light	Heavy
Volume	Small	Large
Self-discharge rate	Low	High

Lithium-ion was selected. On a vehicle where the battery is a significant fraction of kerb mass, gravimetric energy density dominates the selection, and the low self-discharge rate matters for a machine that stands idle between short trips.

4. Design calculations

All calculations assume level ground, a kerb mass of 52 kg, a rider mass of 62 kg, and a target top speed of 10 km h⁻¹ over a representative 50 m run.

4.1. Tractive resistance and starting torque

The rolling resistance opposing motion is

$$F_r = C_r\, m\, g = 0.0046 \times 52 \times 9.81 = 2.35 \text{ N}$$

where C_r is the coefficient of rolling resistance, m the vehicle mass and g the acceleration due to gravity. Acting at the effective rolling radius of 0.355 m, this gives a road-load torque of

$$T_r = F_r\, r = 2.35 \times 0.355 = 0.83 \text{ N m}$$

The inertial torque required to accelerate the rotating and translating masses from rest was evaluated as 8.44 N m, so the total starting torque demand at the wheel is

$$T_{tot} = 0.83 + 8.44 = 9.27 \text{ N m}$$

International Journal of Engineering Technology and Management Sciences
Website: ijetms.in Issue: 3 Volume No.8 May - June – 2024
DOI:10.46647/ijetms.2024.v08i03.079 ISSN: 2581-4621

The inertial term dominates by an order of magnitude, which is characteristic of a low-speed vehicle: the design point is set by getting the machine moving, not by sustaining speed.

4.2. Acceleration requirement

For a 50 m run reaching 10 km h^{-1} (2.78 m s^{-1}) from rest, with $s = ut + \frac{1}{2} a t^2$ and $v = u + a t$ and $u = 0$, the run is completed in t = 36 s at

$$a = 2s / t^2 = 2 \times 50 / 36^2 = 0.077 \text{ m s}^{-2}$$

The corresponding terminal velocity, $a t = 0.077 \times 36 = 2.78$ m s^{-1}, confirms that the acceleration and top-speed targets are mutually consistent.

4.3. Motor selection and shaft torque

A 250 W, 24 V brushless DC motor was selected, with a no-load shaft speed of 1250 rpm. Shaft torque follows from

$$P = 2\pi N T / 60, \text{ hence } T = 60 P / (2\pi N)$$

Evaluated at the rated output of 250 W, this gives 1.91 N m at the no-load speed of 1250 rpm, 4.77 N m after the 2.5:1 internal reduction at 500 rpm, and 79.6 N m at the 30 rpm condition used in the original design worksheet. The value of 79.6 N m at 30 rpm greatly exceeds the 9.27 N m starting requirement of Section 4.1, so the motor is not torque-limited at the wheel once the chain reduction of Section 4.6 is applied; it is limited instead by the current the controller and pack will deliver.

4.4. Battery sizing and runtime

A 24 V lithium-ion pack of 14.4 A h was specified. The current drawn at rated motor power is

$$I = P / V = 250 / 24 = 10.42 \text{ A}$$

Lithium-ion cells are conventionally discharged to about 60% of nameplate capacity to preserve cycle life [9], giving an effective capacity of

$$C_{eff} = 0.6 \times 14.4 = 8.64 \text{ A h}$$

and a continuous full-power runtime of

$$t = C_{eff} / I = 8.64 / 10.42 = 0.83 \text{ h (50 min)}$$

This is a lower bound. Traction on a campus vehicle is intermittent, and at a realistic 40–50% duty cycle the same pack supports roughly 1.7–2.1 h of use between charges.

4.5. Conductor sizing

Copper was selected for the power conductors on grounds of availability, conductivity and cost, with a resistivity $\rho = 1.79 \times 10^{-8}$ Ω m. Allowing a 2% voltage drop on the 24 V bus at the 9 A peak current gives

$$\Delta V = 0.02 \times 24 = 0.48 \text{ V}$$

$$R = \Delta V / I = 0.48 / 9 = 0.053 \ \Omega$$

Referred to the AWG table for copper, this corresponds to AWG 10, a conductor diameter of 2.59 mm.

4.6. Drivetrain ratio, wheel size and road speed

Rear-wheel drive was selected over front-wheel drive to keep the steered front wheel free of drive torque and to place the motor mass over the driven axle. Wheel diameters were fixed from the height of the centre of gravity, the height of obstacles to be negotiated, the rotational speed at the target road speed, and the load capacity of the available wheels; a front wheel smaller than the rear pair produces a negative approach angle that lowers the centre of gravity and improves stability.

In the as-built machine the motor drives an 11-tooth sprocket and the rear axle carries a 28-tooth sprocket, a reduction of 2.545:1 following a 2.5:1 internal reduction in the motor. With rear wheels of 9 in (0.229 m) diameter, circumference 0.718 m, the wheel speed and road speed at no load are

$$N_v = 1250 / (2.5 \times 2.545) = 196 \text{ rpm}$$

$$v = N_v \times \pi d \times 60 / 1000 = 196 \times 0.718 \times 60 / 1000 = 8.5 \text{ km h}^{-1}$$

The predicted no-load road speed of 8.5 km h^{-1} falls 15% short of the 10 km h^{-1} target, a shortfall attributable entirely to the substitution of the as-built 11:28 sprocket pair and 9 in wheels for the 16:42 pair and 8 in wheels of the design case. Table 5 collects the principal design parameters.

International Journal of Engineering Technology and Management Sciences
Website: ijetms.in Issue: 3 Volume No.8 May - June – 2024
DOI:10.46647/ijetms.2024.v08i03.079 ISSN: 2581-4621

Table 5. Principal design parameters of the solar-assisted electric scooter.

Parameter	Value	Unit
Kerb mass	52	kg
Rider mass (design)	62	kg
Design gross mass	114	kg
Coefficient of rolling resistance	0.0046	–
Target top speed	10	km h^{-1}
Total starting torque	9.27	N m
Design acceleration	0.077	m s^{-2}
Motor rating	250 W, 24 V BLDC	–
Motor no-load speed	1250	rpm
Internal reduction	2.5:1	–
Chain reduction (as built)	11:28 (2.545:1)	–
Battery	Li-ion, 24 V, 14.4 A h	–
Rated current draw	10.42	A
Continuous full-power runtime	0.83	h
Power conductor	AWG 10 copper (2.59 mm)	–
Frame envelope (as built)	900 × 300	mm
Frame section	25.4 × 25.4 square hollow	mm
Rear track	457 (18 in)	mm
Turning radius	610 (24 in)	mm

5. Prototype fabrication

The system architecture of the fabricated prototype is shown in Fig. 1. Two power paths meet at the motor: an electrical path running from the photovoltaic module through the solar charge controller to the battery and thence, under throttle command, through the PWM motor controller; and a mechanical path from the motor shaft through the chain drive to the rear wheels.

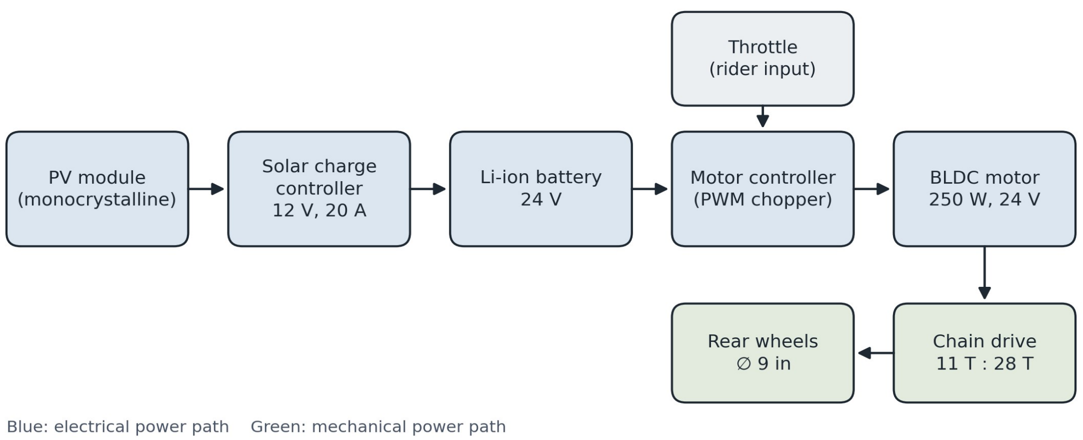

Fig. 1. System architecture of the solar-assisted electric scooter.

International Journal of Engineering Technology and Management Sciences
Website: ijetms.in Issue: 3 Volume No.8 May - June – 2024
DOI:10.46647/ijetms.2024.v08i03.079 ISSN: 2581-4621

5.1. Frame

The frame is a closed rectangular structure of 900 mm × 300 mm, fabricated from 25.4 mm square hollow AISI 1020 tube selected in Section 3.2. All members are joined by GMAW. An approach angle is built into the front of the frame to lower the centre of gravity and improve stability. Motor and battery mountings are welded to the left and right of the front section respectively, so that their masses balance about the longitudinal axis, and the rear wheel mountings are formed from the same section at the rear end. The completed frame is shown in Fig. 2.

Fig. 2. Welded AISI 1020 frame before assembly.

5.2. Wheel and steering assembly

The front wheel is a 3 in castor wheel whose 360° swivel was locked by welding so that it steers only with the handlebar. It is welded from above to the steering column. Being smaller than the rear pair, it produces the negative approach angle referred to in Section 4.6. The rear wheels are a pair of 9 in plastic wheels with rubber tyres, carried on axles in mountings of 25.4 mm square AISI 1020 section, at a track of 457 mm.

The steering unit comprises a handlebar, a steering column and a ball-bearing element that lowers friction and allows smooth rotation. The handlebar is mild steel tube of 25.4 mm diameter and 2 mm wall thickness. Castor, camber and toe were all set to zero during fabrication, and the resulting turning radius measured at the outer wheel is 610 mm. The assembled front and rear wheel units are shown in Fig. 3.

Fig. 3. Front wheel and steering assembly.

DOI:10.46647/ijetms.2024.v08i03.079 ISSN: 2581-4621

5.3. Chain drive

Power is transmitted to the rear axle by a single chain running over two sprockets. The 11-tooth input sprocket is fixed concentrically to the motor shaft by a bolt on its axle; the 28-tooth output sprocket is welded to a collar fixed to the rear wheel. The rear wheel shaft is coupled directly to the motor shaft through this pair, giving the 2.545:1 reduction used in Section 4.6. The installed drive is shown in Fig. 4.

Fig. 4. Rear wheel and chain drive mechanism.

5.4. Electrical and photovoltaic subsystem

The electrical unit comprises the motor, the motor controller, the throttle, the battery, the solar charge controller and the photovoltaic module.

The traction motor (Fig. 5) is the 250 W, 24 V brushless machine of Section 3.4, with a no-load shaft speed of 1250 rpm reduced internally by approximately 2.5:1. Its mounting is fabricated from L-section and welded in front of the left wheel, with the wheel shaft fixed so that the wheel turns freely about it.

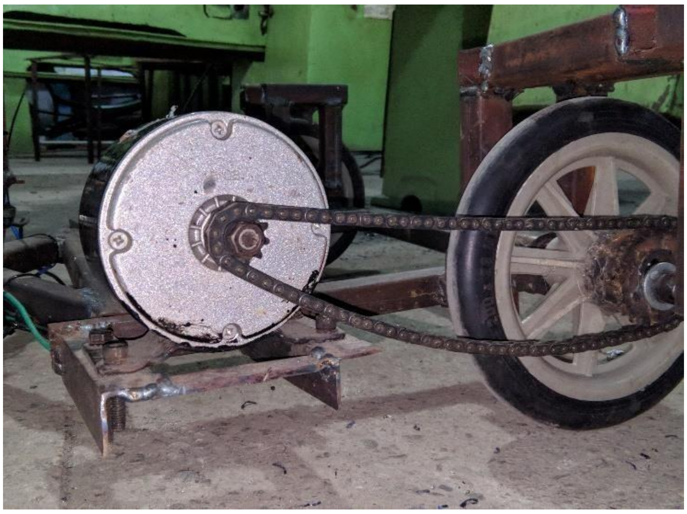

Fig. 5. Brushless DC traction motor, 250 W, 24 V.

The battery installed on the prototype is a 24 V, 10 A h unit of the type used on motorcycles, mounted at the front of the frame opposite the motor on a 1.5 mm mild steel L-section bracket of 25.4 mm flange width, clamped by bolts and welded to the frame by GMAW.

The motor controller (Fig. 6) connects the pack to the motor and sets the balance between torque and speed. Torque is regulated through armature current and speed through armature voltage, the latter by chopping the supply so that the ratio of on-time to off-time fixes the mean voltage; either the number of constant-width pulses per unit time or their duration may be varied. Chopping is

International Journal of Engineering Technology and Management Sciences
Website: ijetms.in Issue: 3 Volume No.8 May - June – 2024
DOI:10.46647/ijetms.2024.v08i03.079 ISSN: 2581-4621

performed by diodes, thyristors and silicon-controlled rectifiers, and controller efficiency in this class of device typically exceeds 90%.

Fig. 6. PWM motor controller as installed.

Photovoltaic charging is managed by a 20 A pulse-width-modulated solar charge controller with automatic 12 V / 24 V battery selection, a stated conversion efficiency of 98%, low-voltage disconnect and a USB DC output. It limits the rate at which charge is delivered to the pack, prevents overcharging and overvoltage, and blocks reverse current flow from the battery into the module after dark.

The photovoltaic module is a monocrystalline silicon panel mounted on the deck. Commercial monocrystalline modules convert 15–20% of incident irradiance, with premium products exceeding 22%; monocrystalline was preferred over polycrystalline for its higher conversion efficiency per unit area, which is the binding constraint on a vehicle where deck area is fixed, and over thin film for the same reason.

6. Results and discussion

6.1. Reconciliation of the design case and the as-built machine

The prototype was built to a reduced scale after the full-size design proved infeasible within the available budget, and several parameters changed between the design worksheet and the finished machine. Table 6 sets them side by side.

Table 6. Design case compared with the as-built prototype.

Parameter	Design case	As built	Unit
Driver sprocket	16	11	teeth
Driven sprocket	42	28	teeth
Chain reduction	2.625:1	2.545:1	–
Front wheel diameter	4	3	in
Rear wheel diameter	8	9	in
Battery capacity	14.4	10	A h
Frame envelope	1090 × 410	900 × 300	mm
Full-power runtime	0.83	0.58	h

Three of these changes matter. The reduction in installed pack capacity from 14.4 to 10 A h cuts the continuous full-power runtime from 0.83 h to 0.58 h, since the effective capacity falls to 0.6 × 10 = 6.0 A h against the same 10.42 A draw. The change in sprocket pair and rear wheel diameter together shift the predicted no-load road speed to 8.5 km h^{-1}. The reduction of the frame envelope

International Journal of Engineering Technology and Management Sciences
Website: ijetms.in Issue: 3 Volume No.8 May - June – 2024
DOI:10.46647/ijetms.2024.v08i03.079 ISSN: 2581-4621

from 1090 mm × 410 mm to 900 mm × 300 mm reduces the deck area available for the photovoltaic module by roughly 40%, which is the binding constraint on the energy analysis of Section 6.3.

A discrepancy in the original worksheet should also be recorded. The road speed calculation was performed with a tyre radius of 0.33 m, which corresponds to a wheel of approximately 26 in diameter and is inconsistent with both the 8 in design wheel and the 9 in as-built wheel; the 3.1 km h^{-1} result it produces is therefore not a valid prediction for this machine. The shaft torque of 9.54 N m quoted at 30 rpm is likewise inconsistent with $P = 2\pi NT/60$, which gives 79.6 N m at that speed; 9.54 N m corresponds instead to 250 rpm. Both figures have been recomputed in Section 4.

6.2. Predicted performance envelope

Combining the corrected values, the machine as built is predicted to reach 8.5 km h^{-1} unloaded, to draw 10.42 A at rated motor power, and to run for 0.58 h continuously at that draw on the installed 10 A h pack, corresponding to a continuous full-power range of approximately 4.9 km. Restoring the designed 14.4 A h pack raises this to 0.83 h and approximately 7.1 km. These are conservative bounds: they assume the motor is held at rated output throughout, whereas a campus duty cycle involves frequent stops and part-throttle running at 40–50% of rated power, under which the same pack supports roughly 10–14 km.

Available wheel torque is not the constraint. With 79.6 N m at the 30 rpm design condition against a 9.27 N m starting requirement, the machine has substantial reserve for starting on a gradient or with a heavier rider; the practical limits are pack current and thermal capacity of the controller.

6.3. Contribution of photovoltaic assistance

Kadapa receives global horizontal irradiance of approximately 5.5 kWh m^{-2} day^{-1} averaged over the year, among the higher values in peninsular India. For a deck-mounted module of 30–50 Wp — the range that fits the 900 mm × 300 mm deck of the prototype — the gross daily yield is 165–275 W h. Applying a combined module-soiling, temperature, controller and charge-acceptance derating of 0.85 gives a net delivered energy of

E_{net} = 140 to 234 W h day^{-1}

against a designed pack energy of 24 × 14.4 = 345.6 W h. On-board photovoltaic generation therefore replaces 41–68% of a full charge per day, or equivalently 0.56–0.94 h of operation at rated motor power. This is a material contribution for a vehicle whose entire useful duty is under an hour of full-power running, and it is the direct consequence of the favourable area-to-power ratio noted in Section 1: the same calculation applied to a passenger car would recover well under 5% of daily demand.

Two qualifications apply. The estimate assumes the deck is unshaded and approximately horizontal, which holds when the vehicle is parked in the open but not under a canopy or between buildings; and a 50 Wp module with its frame adds approximately 4 kg, about 8% of kerb mass, which slightly raises the tractive load computed in Section 4.1. Neither qualification changes the conclusion that the module is worth carrying on this vehicle class.

6.4. Assessment and limitations

The prototype achieves its principal functional objectives. It produces no tailpipe emissions and is therefore usable indoors and in areas where contamination from exhaust gases is unacceptable; it is suitable for short-distance movement within campuses, factories and comparable premises; and its stand-on deck accommodates riders of different heights without adjustment, unlike a seated machine. The predictable riding surface it presents is easier to negotiate than a pavement or trail, which reduces the risk of tripping for the user it replaces on foot.

The limitations are equally clear. Sudden application of the brakes produces jerking, a consequence of the direct chain coupling and the absence of any compliance or progressive braking in the drivetrain, and this is the most safety-relevant defect in the present build. Range remains modest, and abrupt voltage collapse of the pack in mid-journey — the failure mode most often reported by users of vehicles in this class — is not currently signalled to the rider, since no state-of-charge display is fitted. The vehicle is not suitable for long-distance travel.

Four improvements follow directly. First, a state-of-charge indicator and low-voltage warning derived from the charge controller's existing low-voltage disconnect would address the most disruptive failure mode at negligible cost. Second, restoring the designed 14.4 A h pack and adopting the 16:42 sprocket pair would recover both the runtime and the 10 km h^{-1} target. Third, replacing the mild steel frame with CFRP, at the cost premium quantified in Section 3.2, would reduce kerb mass and improve both range and handling. Fourth, a regenerative or mechanically compliant coupling would remove the braking jerk. Beyond the present configuration, a dynamo generator driven from the wheel could recover a small additional increment of energy during descent and braking, complementing rather than replacing the photovoltaic input.

7. Conclusions

A solar-assisted three-wheel electric scooter for short-distance campus mobility was designed, fabricated and assessed. The principal findings are as follows.

(1) For a 114 kg design gross mass on level ground with $C_r = 0.0046$, the road-load torque is 0.83 N m and the total starting torque requirement is 9.27 N m, of which the inertial term contributes 91%. The design point for a vehicle of this class is set by starting, not by sustained running.

(2) AISI 1020 square hollow section joined by GMAW is the appropriate frame combination at this scale. Neither the heat-treatment response of AISI 4130 nor the specific strength of CFRP is recoverable against their cost and, in the case of CFRP, their incompatibility with welded fabrication.

(3) A 250 W, 24 V brushless DC motor with 2.5:1 internal reduction and an 11:28 chain drive gives a predicted no-load road speed of 8.5 km h^{-1} on 9 in rear wheels, 15% below the 10 km h^{-1} target; the shortfall is traceable entirely to the substitution of the as-built sprocket pair and wheel diameter for those of the design case.

(4) The 24 V lithium-ion pack, discharged to 60% of nameplate capacity, supports 0.83 h of continuous full-power operation at 14.4 A h and 0.58 h at the 10 A h capacity actually installed, corresponding to continuous full-power ranges of approximately 7.1 km and 4.9 km respectively. Power conductors of AWG 10 copper hold the bus drop to 2% at 9 A.

(5) On-board photovoltaic generation is worth carrying on this vehicle class. A 30–50 Wp deck-mounted module at the site irradiance of 5.5 kWh m^{-2} day^{-1} delivers a net 140–234 W h per day, 41–68% of the designed pack energy, because the ratio of available deck area to traction power is roughly an order of magnitude more favourable than for a passenger car.

The immediate priorities for further work are a state-of-charge indicator, restoration of the designed pack capacity and sprocket ratio, and elimination of the braking jerk through a compliant or regenerative coupling.

8. References

[1] C.R. Ajan, K. Ajay Sugadan, A. Balachandran, R. Antoni, C.R. Renji, Walking bike, International Journal of Innovative Research in Advanced Engineering (IJIRAE) 4 (10) (2017). ISSN 2349-2163.

[2] P.R. Gajbhiye, D.G. Dange, S.C. Hingnekar, R.V. Kondalwar, N. Jamal, M.G. Sonwane, M.G. Shete, Design and fabrication of treadmill cycle, International Journal of Advance Research, Ideas and Innovations in Technology (IJARIIE) 3 (2) (2017). ISSN(O) 2395-4396.

[3] J. Barade, A. Janwe, K.A. Nawab, S. Khan, Treadmill bicycle, International Research Journal of Engineering and Technology (IRJET) 4 (3) (2017). e-ISSN 2395-0056, p-ISSN 2395-0072.

[4] S.R. Deshmukh, N.V. Sanap, R.E. Dhoble, Design of walking bike, International Journal of Innovative Research in Science and Engineering 2 (5) (2016). ISSN 2454-9665.

[5] V. Ahire, N. Patel, D. Amin, H. Barot, Fabrication of walking cycle, International Research Journal of Engineering and Technology (IRJET) 3 (5) (2016).

[6] A. Ansari, N. Raza, F. Sameer, Z. Shaikh, A. Rashid, Treadmill bike, International Journal of Modern Trends in Engineering and Research (2016) 28–30 April. e-ISSN 2349-9745.

DOI:10.46647/ijetms.2024.v08i03.079 ISSN: 2581-4621

[7] K. Bondre, S. Beradpatil, S.J. Thorat, Design and fabrication of treadmill bicycle, International Journal of Innovative Research in Science, Engineering and Technology 5 (6) (2016).
[8] Navigant Research, Electric Motorcycles and Scooters: Market Forecasts 2015–2024, market report, Navigant Consulting, Boulder, CO, 2015.
[9] H.J. Bergveld, Battery Management Systems: Design by Modelling, Kluwer Academic Publishers, Dordrecht, 2002.
[10] V.B. Bhandari, Design of Machine Elements, third ed., Tata McGraw Hill Education, New Delhi, 2010.
[11] J.V. Woodworth, Manufacturing Processes, McGraw-Hill, New York, 1941.